ISBN: 978-3-95450-184-7 doi:10.18429/JACoW-IPAC2018-THPAK045

SUMMARY OF BEAM OPERATION CAPABILITY AT FXR LIA

Yuan Hui Wu† and Jennifer Ellsworth
Lawrence Livermore National Laboratory, CA, USA

Abstract

In this paper, we summarize the current beam operation capability of FXR linear induction accelerator (LIA) at LLNL [1][2]. Experimental measurements for electron beam parameters at different beam operations are presented.

CURRENT FXR LIA CAPABILITY

Table 1: Summary of Current FXR Beam Operation Capability and Its Electron Beam's Parameters.

Beam Operation Mode	Energy (MeV)/ Peak Current (kA)	Dose (R)/ LSF FWHM (mm) @ target	Bunch length (flat-top)
Single pulse (standard cathode)	18/2.8	450/ ~ 1.5	~ 50nsec
Single pulse (reduced cathode)	18/1.1	240/~ 0.8	~ 55nsec
Double pulse (standard cathode)	9/1.8	40 for each pulse/ ~ 1.5	~ 55nsec
Double pulse (reduced cathode)	9/0.8	N/A	~ 55nsec

Table 1 is a summary of the electron beam can be produced by the FXR LIA. The current FXR can operate at four different modes. Each mode is operating at different acceleration scheme and with different cathode velvet size.

FXR injector produces electron through velvet cathode, we commonly call it as cold cathode injector. For these modes of beam operation, the small cathode has velvet size of ~ 30mm in diameter and the standard cathode has velvet size of ~ 56 mm in diameter. The X-ray dose at the target is measured by Mucaddix diamond detector and the beam spot size at the target is measured by the roll-bar technique. Noted that the x-ray dose for double pulse/standard cathode is only 40R compare to the 240R measured for the single pulse/reduce cathode experiment. This consistent with that the X-ray dose is proportional to energy (γ) and peak current (I) $D \propto I\gamma^{-3}$ [3].

As shown in Fig.1, for single pulse operation, a single electron beam is produced by activated all the accelerator induction cells to achieved maximum energy gain of ~ 18 MeV. For double pulse beam operation, two electron pulses are produced with inter-pulse spacing > 0.8 μs. To accelerate two electron beams, the accelerator is configurated such a way each pulse is accelerated by half of the accelerating cell in the FXR LIA. Each pulse has energy gain of ~9MeV at the accelerator exit.

BEAM EMITTANCE

Electron beam emittance is one of the key parameters to estimate the performance of beam transport. To design the magnetic tune for beam transport in FXR LIA, we model the FXR injector using TRAK [4][5]. Using the beam distribution output from TRAK, we then use AMBER particle slice code [6] to simulate the beam transport in the accelerator section. For each mode of beam operations, we unfold the beam emittance through solenoid scan. The unfolded beam emittances are listed in Table 2.

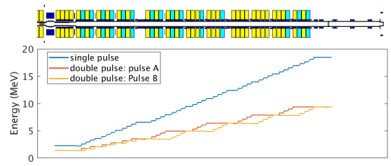

Figure 1: Accelerating scheme of the single pulse and the double pulse beam operation.

Table 2: Summary of Unfolded Electron Beam Emittance for Each Beam Operation Mode.

Beam Operation Mode	Measured normalized emittance by solenoid scan (mm-mrad)
Single pulse (standard cathode)	~ 1300
Single pulse (reduced cathode)	~ 800
Double pulse (standard cathode)	~1050 for both pulse
Double pulse (reduced cathode)	~ 500 for both pulse

BEAM CURRENT AND ENERGY PROFILE

Beam position monitors (BPMs) and cell voltage monitors (CVMs) along the LIA are used for monitoring the beam current and accelerator voltage in real time. Experiment data from these diagnostics have shown the FXR LIA can produce a highly repeatable electron beam with similar current and energy profile at every shot.

For double pulse experiment, experiment data shown the inter-pulse spacing between the first electron beam and second electron beam need to be greater than 0.8 μs, significant beam quality deterioration for the second pulse if the inter-pulse spacing less than 0.8 μs. The experimental data shown below for double pulse are with an inter-pulse spacing of 1.8 μs.

Figure 2, 3, 4 and 5 are the measured current profiles at the injector exit for different beam operation modes. The inserted plot is the magnification of the current profile. The inserted table includes beam parameters calculated for electron flat-top bunch length, FWHM bunch length, peak current and current variation of the flat-top section.

Figures 6, 7, 8 and 9 are the sum of all induction cells' voltage along the accelerator for different beam operation modes. The inserted plot is the magnification of the voltage profile. The inserted table includes beam parameters calculated for voltage waveform flat-top, voltage waveform FWHM, peak voltage and voltage variation of the voltage waveform flat-top section.

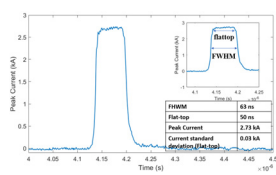

Figure 2: Beam current profile measured for single pulse/standard cathode beam operation.

ISBN: 978-3-95450-184-7 doi:10.18429/JACoW-IPAC2018-THPAK045

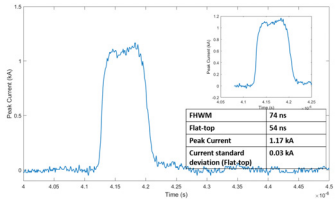

Figure 3: Beam current profile measured for single pulse/reduced cathode beam operation.

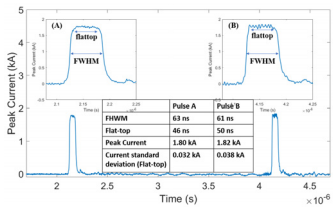

Figure 4: Beam current profile measured for double pulse/standard cathode beam operation.

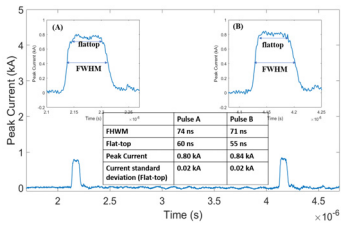

Figure 5: Beam current profile measured for double pulse/ reduced cathode beam operation.

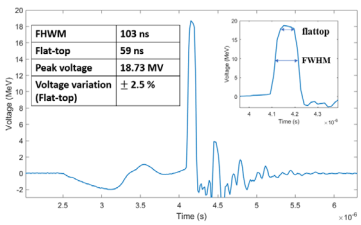

Figure 6: Sum of all induction cells' voltage profiles along accelerator for single pulse/standard cathode beam operation.

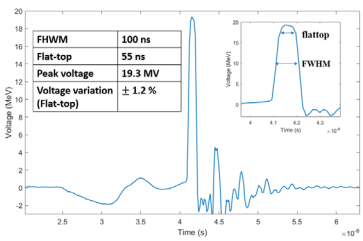

Figure 7: Sum of all induction cells' voltage profiles along accelerator for single pulse/ reduced cathode beam operation.

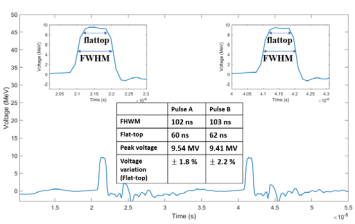

Figure 8: Sum of all induction cells' voltage profiles along accelerator for double pulse/standard cathode beam operation.

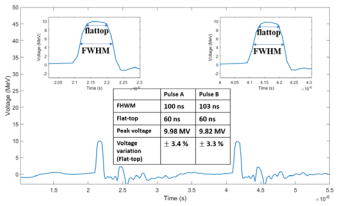

Figure 9: Sum of all induction cells' voltage profiles along accelerator for double pulse/ reduced cathode beam operation.

LOW-FREQUENCY TRANSVERSE MOTION

Low-frequency beam transverse motion such as corkscrew motion is monitoring by BPMs along the FXR LIA. The existing BPMs at FXR can measure bandwidth up to 1GH. During beam tuning experiment, we want to minimize beam corkscrew at the accelerator exit. To correct for the Corkscrew motion, few sets of dipole steering corrector were used in the accelerator section [7].

The standard deviation of the beam centroid in x and y-direction $\delta\langle x\rangle$ and $\delta\langle y\rangle$ with respect to the average centroid motion <x> and <y> are

$$\delta\langle x\rangle = \sqrt{\frac{1}{n}\sum_{i=1}^{n}(x_1 - \langle x\rangle)^2 + (x_2 - \langle x\rangle)^2 + \cdots + (x_n - \langle x\rangle)^2} \quad (1)$$

$$\delta\langle y\rangle = \sqrt{\frac{1}{n}\sum_{i=1}^{n}(y_1 - \langle y\rangle)^2 + (y_2 - \langle y\rangle)^2 + \cdots + (y_n - \langle y\rangle)^2} \quad (2)$$

Where x_n and y_n is the beam centroid of the indvidual slice at the flat-top section of the electron beam. The Amplitude of Corkscrew Motion A is defined as

$$A^2 = \delta\langle x\rangle^2 + \delta\langle y\rangle^2 \quad (3)$$

As shown in Figs. 10, 11, 12 and 13, we measured beam centroid motion at the accelerator exit for different beam operation modes after using steering dipole corrector. The inserted table lists the standard deviation of the beam centroid of the flat-top section of the electron beam. The corkscrew amplitude is ~0.42 mm for single pulse operation and ~1 mm for double pulse beam operation, which is < 5% of the beam spot size at the accelerator exit.

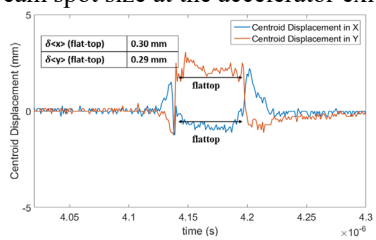

Figure 10: Measured beam centroid motion for single pulse/standard cathode beam operation.

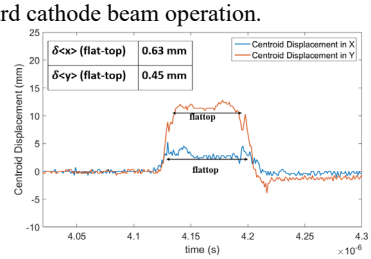

Figure 11: Measured beam centroid motion for single pulse/ reduced cathode beam operation.

ISBN: 978-3-95450-184-7 doi:10.18429/JACoW-IPAC2018-THPAK045

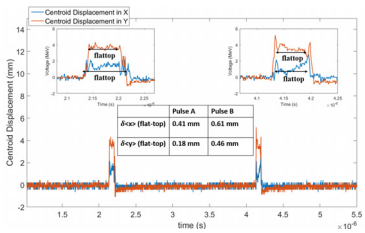

Figure 12: Measured beam centroid motion for double pulse/standard cathode beam operation.

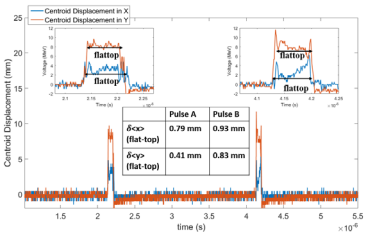

Figure 13: Measured beam centroid motion for double pulse/ reduced cathode beam operation.

HIGH-FREQUENCY TRANSVERSE MOTION

There are four magnetic probes (B-dot) locating along FXR accelerator to monitor high-frequency centroid motion induced by the Beam breakup instability. Existing B-dots at FXR have not calibrated to measure the high-frequency centroid motion, we can interpret the BBU growth through the accelerator by calculating the Fourier amplitude of B-dot signals.

Figures 14, 15, 16, 17, 18 and 19 are the measured B-dot signals and their Fourier amplitude at three different location: injector exit (A), middle of the accelerator (B), accelerator exit (C). As indicated from the figures for different beam operation modes, the electron beam has the largest Fourier amplitude at a frequency of ~800 MHz, this is consistent with the simulations and experiments performed for the FXR induction cell [8].

Furthermore, these figures also showed that the single pulse/standard cathode has highest BBU amplitude along the accelerator, and double pulse/reduced cathode has lowest BBU amplitude along the accelerator. This is consistent with the beam intensity operated at these modes.

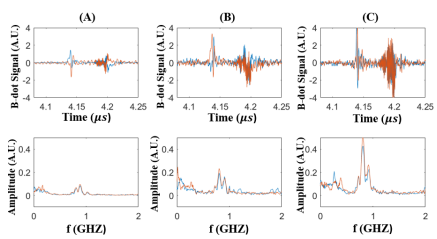

Figure 14: B-dot signals (top) and their Fourier amplitudes (bottom) for single pulse/standard cathode operation.

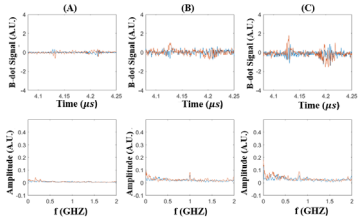

Figure 15: B-dot signals (top) and their Fourier amplitudes (bottom) for single pulse/ reduced cathode operation.

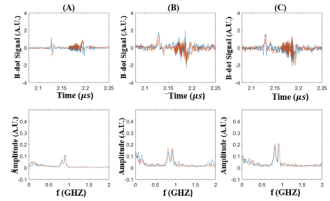

Figure 16: B-dot signals (top) and their Fourier amplitudes (bottom) for double pulse/standard cathode operation/pulse A.

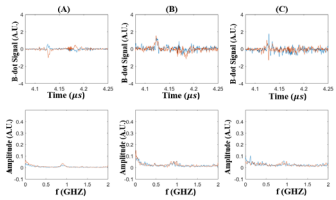

Figure 17: B-dot signals (top) and their Fourier amplitudes (bottom) for double pulse/standard cathode operation/pulse B.

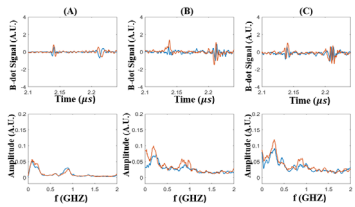

Figure 18: B-dot signals (top) and their Fourier amplitudes (bottom) for double pulse/ reduced cathode operation/pulse A.

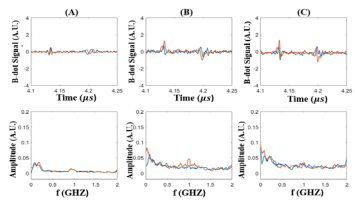

Figure 19: B-dot signals (top) and their Fourier amplitudes (bottom) for double pulse/ reduced cathode operation/pulse B.

SUMMARY

We have evaluated the current beam operation capability at FXR LIA. Important measured beam parameters have been discussed.

ACKNOWLEDGMENTS

This work was performed under the auspices of the U.S. Department of Energy by Lawrence Livermore National Laboratory under Contract DE-AC52-07NA27344.

ISBN: 978-3-95450-184-7 doi:10.18429/JACoW-IPAC2018-THPAK045

REFERENCES

[1] M. Ong *et al*., "LNL Flash X-ray Radiography Machine (FXR) Double-Pulse Upgrade Diagnostics", *11th IEEE International Pulse Power Conference*, Baltimore, MD, June 29-July 2, 1997.

[2] L. G. Multhauf, "The LLNL Flash X-Ray Induction Linear Accelerator (FXR)", *25th Conference on High-Speed Photography and Photonics*, Beaune, France, September 12 - October 4, 2002.

[3] Yu-Jiuan Chen, "Physics Design Considerations for Diagnostic X Electron Beam Transport System", UCRL-ID-140189.

[4] Field Precision LLC. © 1998 – 2017.

[5] T. L. Houck, M.M. Ong, and R.D. Pari, LLNL-TR-605934.

[6] J. L. V. a. W. Fawley, "Amber user's Manual".

[7] Jan Zentler, Private Communications.

[8] Scott Nelson, "EM modeling of FXR Accelerator Cell", https://www-eng-x.llnl.gov/dsed/documents/em/sdnfxr.html